1970

MLM-1809

MLM-1809

Metallographic Analysis of Dart II Heat Source Capsule

R. E. Fitzharris, M. D. Kelly and J. E. Selle

September 17, 1971

AEC Research and Development Report

MOUND LABORATORY
Miamisburg, Ohio
operated by

MONSANTO RESEARCH CORPORATION
a subsidiary of Monsanto Company
for the

U. S. ATOMIC ENERGY COMMISSION
U. S. Government Contract No. AT-33-1-GEN-53

Monsanto

DISTRIBUTION OF THIS DOCUMENT IS UNLIMITED

R2212

DISCLAIMER

MLM-1809
TID-4500
UC-25

Metallographic Analysis of Dart II Heat Source Capsule

R. E. Fitzharris, M. D. Kelly and J. E. Selle

Issued: September 17, 1971

LEGAL NOTICE

PRINTED IN THE UNITED STATES OF AMERICA
Available from
National Technical Information Service
U. S. Department of Commerce
5285 Port Royal Road
Springfield, Virginia 22151
Price Printed Copy $3.00, Microfiche $0.95

MONSANTO RESEARCH CORPORATION
A Subsidiary of Monsanto Company

MOUND LABORATORY
Miamisburg, Ohio 45342

operated for

UNITED STATES ATOMIC ENERGY COMMISSION
U S Government Contract No AT-33-1-GEN-53

TABLE OF CONTENTS

ABSTRACT

A complete metallographic analysis of the DART II heat source capsule was performed. The purpose of the analysis was to determine the extent of any reaction between various components of the capsule.

The diffusion of the fuel into the liner interface reached a maximum of 90 μm. The impurities in the fuel diffused into the liner to form intermetallic compounds. An increase in hardness of the tantalum-10% tungsten resulted from absorption of oxygen released from the decomposition of the fuel.

INTRODUCTION

In cooperation with the United States Air Force and TRW Systems, the DART II experimental space thruster was tested at Mound Laboratory. The DART (Decomposed Ammonia Radioisotope Thruster) II was powered by a 155.95W(t) heat source which consisted of plutonium-238 dioxide microspheres doubly encapsulated in a tantalum-10% tungsten liner and a TZM (a tantalum-zirconium-molybdenum alloy) strength member. TRW Systems designed and built the DART II thruster and heat source components. Mound Laboratory fabricated the fuel ($^{238}PuO_2$ microspheres) and the heat source, and performed the loading and final assembly of the thruster. A photograph of the thruster assembly is shown in Figure 1.

After 18 mo of operation in the thruster at surface temperatures between 800 and 1100°C, the capsule was sectioned and examined metallographically. This report gives the results of this analysis. Electron microprobe analyses and microhardness measurements were also made of the various components. The object of this investigation was to determine the extent of any interactions between the various materials of construction.

On January 9, 1970, the capsule was opened and defueled in the following manner. The capsule was placed in the chuck of a lathe located in an alpha glove box. One end was machined off with capsule rotation varying between 10 and 20 rpm. The sectioned capsule is seen in Figure 2. After the end cap was removed, approximately two-thirds of the fuel readily poured out, while the remaining one-third of the fuel had to be carefully dislodged mechanically. Most of the fuel that was dislodged was in the form of pea size clinkers which easily broke apart. A photograph of the fuel after removal from the capsule is shown in Figure 3. As in the case of the DART I heat source capsule, some of the microspheres fractured; however, the reason for this is not known. Also, as in DART I, the surface of the microspheres was altered during the test and appeared as shown in Figure 4. This surface phenomena is believed to be the result of the thermal faceting. The crush strength of the microspheres removed from the capsule was not determined in this case. However, past experience has shown that there is no change in the crush strength of the microspheres removed from the capsule as compared with the crush strength of the microspheres prior to capsule loading. Therefore, this thermal faceting has no apparent adverse effect on the integrity of the microspheres.

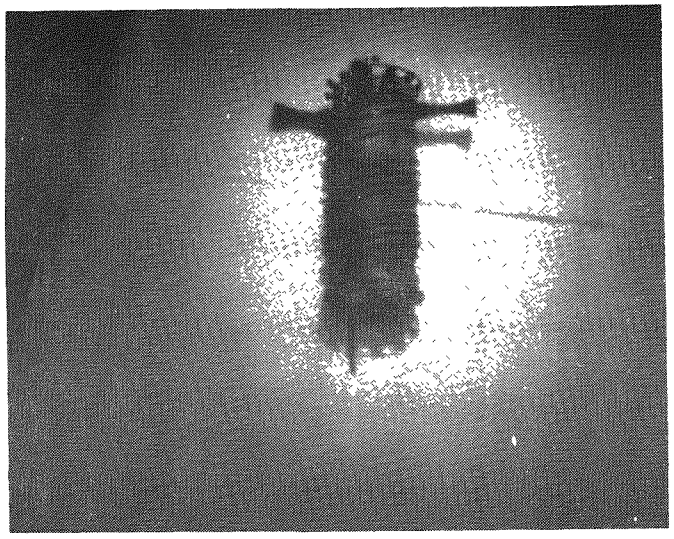

FIGURE 1 - The DART II thruster assembly.

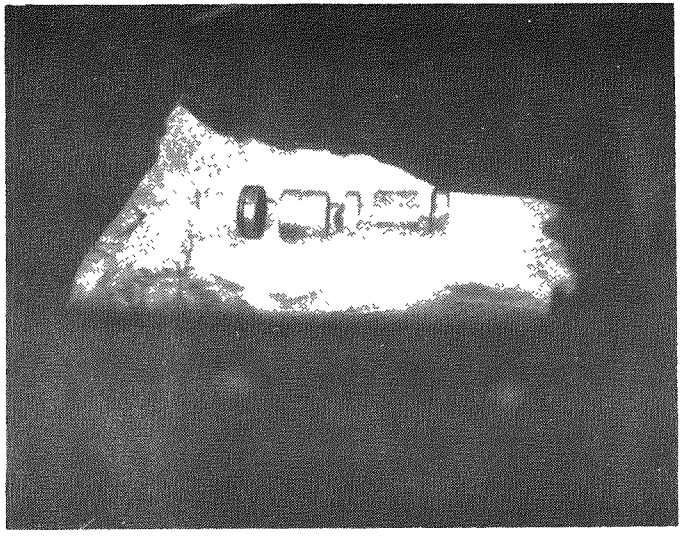

FIGURE 2 - Sectioned heat source capsule.

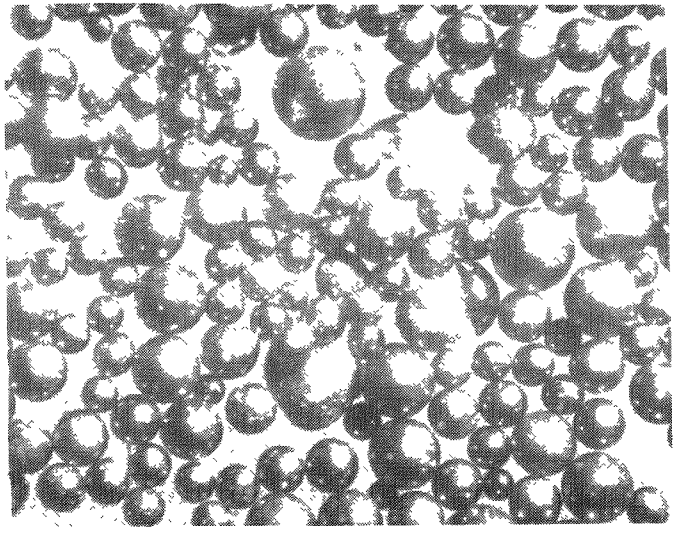

FIGURE 3 - Photograph of PuO_2 microspheres after removal from the DART II heat source capsule. 50X

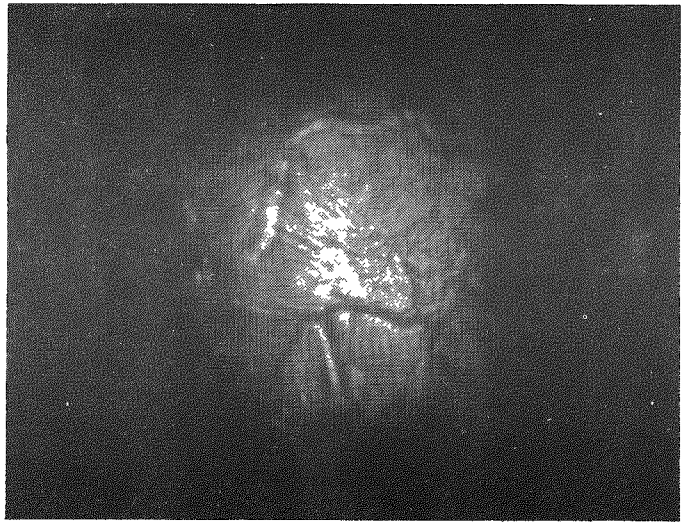

FIGURE 4 - Surface of a PuO_2 microsphere showing thermal faceting.

Table 1

DART II FUEL ANALYSIS

Element	Amount (wt % as Metal) DART I Fuel	SNAP-19-370 Fuel
Ni	0.03	0.07
Fe	0.16	0.20
Al	0.24	0.10
Ca	0.02	0.08
B	0.12	0.10
P	0.14	----
Cr	0.07	0.05
Cu	0.05	0.07
Co	0.05	----
Si	0.16	0.02
Ti	----	0.05
Zn	----	0.07
Total Impurities	1.04	0.81

The materials of construction of the DART II capsule are: inner liner - tantalum-10% tungsten alloy; strength member - TZM alloy (molybdenum-0.5%, titanium-0.08%, zirconium); clad - platinum; internal fin - tantalum-10% tungsten alloy. All of the interfaces of the capsule were studied with the exceptions of the strength member - clad interface, and the exterior of the clad.

The DART II liner was loaded with 106.838W(t) ± 0.5% of reclaimed DART I fuel and 49.68W(t) ± 0.4% of SNAP-19-370 fuel ($^{238}PuO_2$ microspheres). An analysis of the microspheres prior to loading is given in Table 1. As indicated in this table, the primary impurities are Fe, Al, P, and Si. No analysis of the fuel was made after it was removed from the capsule.

PROCEDURE

Sectioning was done in an alpha glove box using a Hardinge lathe and a rotary cut-off wheel with a 90 grit aluminum oxide blade. The end cap and a cross section of the girth of the capsule, as shown in Figure 2, were machined off using the lathe. The inside and outside diameters were measured in several places, as shown schematically in Figure 5, to ascertain whether any swelling of the capsule had occurred. These data are summarized in Table 2. Samples were then extracted, utilizing a rotary cut-off wheel, from the predetermined areas indicated schematically in Figure 5. These sections were vacuum impregnated with Buehler's Plastic Epoxide (an epoxy resin) to provide a specimen mount with better adhesion and edge retention characteristics. The specimens were ground on a series of 180, 320, and 600 grit silicon carbide papers employing a Buehler automet polishing head and using carbon tetrachloride as a lubricant.

Rough polishing was done with 1 μm aluminum oxide on Texmet with a water slurry. A final polish of 0.05 μm aluminum oxide on Politex D with a water slurry. These Texmet and Politex D polishing discs are virtually napless chemotextile materials that possess good abrasive and lubricant retention properties. Vibratory polishing was employed for

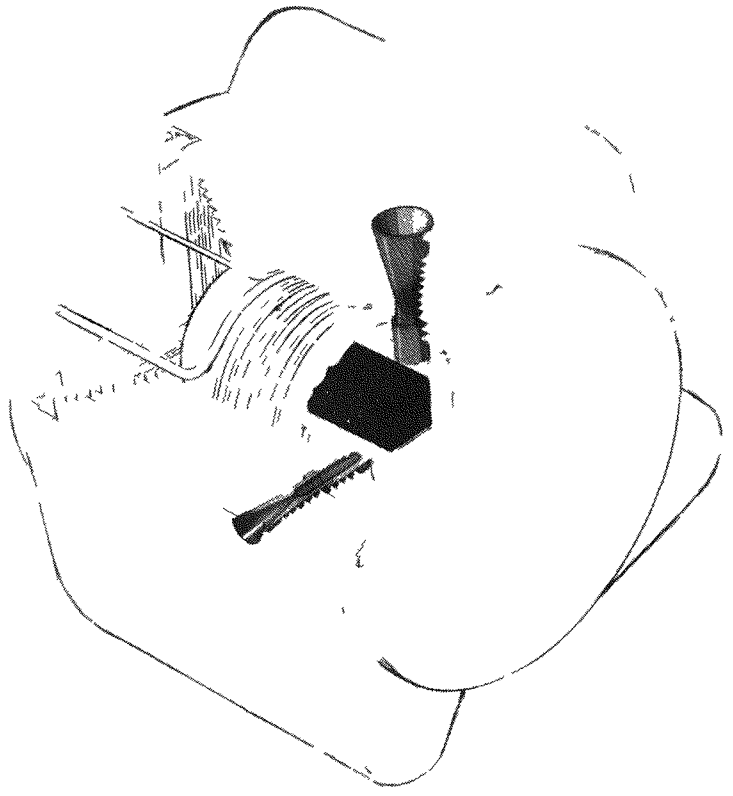

(a)

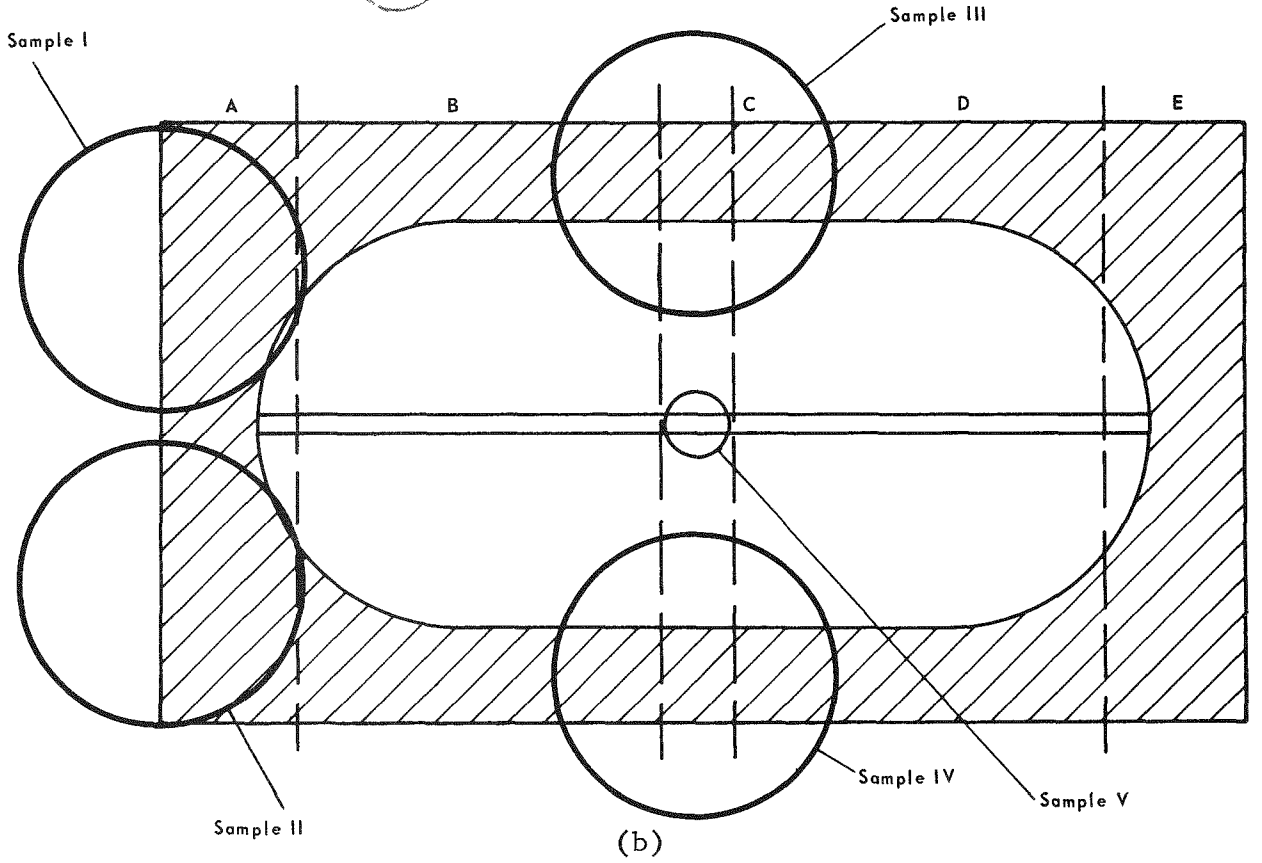

(b)

FIGURE 5 - Schematic of (a) the DART II heat source capsule and (b) sections chosen for diameter measurement and the locations of the samples that were analyzed.

Table 2

DIMENSIONS OF DART II HEAT SOURCE CAPSULE AFTER TEST

	Section Dimensions[a] (mm)				
	Ba	Bc	De	Dc	Start
Inside Diameters (i.d.)	29.7	31.4	30.2	31.5	
	30.0	31.4	30.2	31.3	
	30.1	31.3	30.1	31.0	
Average (i.d.)	29.9	31.4	30.2	31.3	31.24
Outside Diameters (o.d.)	37.5	37.4	37.3	37.3	
	37.1	37.5	37.5	37.4	
	37.4	37.3	37.5	37.4	
Average (o.d.)	37.3	37.4	37.4	37.4	39.3

[a] The designation Ba refers to section B (Figure 5) near the (A) end of the section and Bc refers to section B near the (C) end.

both rough and final polish, which revealed the microstructure through relief, and in general produced excellent results.

Photomicrographs were obtained on a Leitz MM5 metallograph. Electron microprobe analyses were performed on a Hitachi XMA-S electron probe microanalyzer and microhardness measurements were made on a Wilson MO TUKON microhardness tester with a 50-g load.

Electron microprobe analysis consisted ot taking photomicrographs with the aid of back scattered electrons as well as the characteristic x-rays emitted from the sample. X-ray intensity strip chart analyses were made so that a measure of compositional variations was obtained. Microhardness measurements were made in the same areas as the electron probe traverses, not only to measure the change in hardness as a function of distance across the interface, but also to determine the effect of any compositional variation on the relative hardness.

RESULTS

Dimensional Measurements A summary of the dimensional measurements was given in Table 2. From these measurements it appears that no swelling of the capsule took place. The smaller values for i.d. measurements obtained at either end are the result of the fact that the i.d. of each hemispherical end is less than the i.d. of the cylindrical portion.

Ta-10W Fuel Interface A photomicrograph of the tantalum-10% tungsten alloy-fuel interface taken from Sample II is shown in Figure 7. The warped appearance of the surface reaction layer probably results from differences in thermal expansion between the reaction product and the base metal. The greater contraction of the base metal with respect to the oxide layer in the region of plasticity of the oxide layer would explain this structure.

The interface was microprobed; a trace of the x-ray strip chart analysis across that interface is shown in Figure 6. This trace gives a semiquantitative description of the amount of each element as a function of the distance across the interface. The relative displacement of each curve should not be considered as a comparison of the amount of one element with another. This relative displacement is a function of the counting rate and hence is variable. However, for a given element, the changes in displacement of the curve (excluding electronic noise) can be used to indicate changes in composition. The number adjacent to the identification of each curve is the counting rate for that particular element. Different counting rates were used in an attempt to obtain maximum sensitivity and still keep the trace on scale. The higher the counting rate the less sensitive is the scale.

In order to compare the relative magnitude of one element to another, the curve must be normalized with respect to one of the elements. If element B is to be compared with element A the following relationship is used:

$$\frac{\text{counting rate of B}}{\text{counting rate of A}} \times \%\,A = \text{relative amount of B} \qquad (1)$$

It should be emphasized that equation (1) will only give a relative amount of B compared to element A. No allowance is made for variations in wave length between the elements. Quantitative analysis of either element is not possible unless a standard of known composition is used for comparison.

The microprobe strip chart analysis of Figure 6 shows that a maximum plutonium reaction layer of 50 μm was found. Two regions containing different concentrations of plutonium are indicated. The 25 μm reaction layer on the liner side of the interface indicates that plutonium diffused into the liner and the increased amount of plutonium on the fuel side of

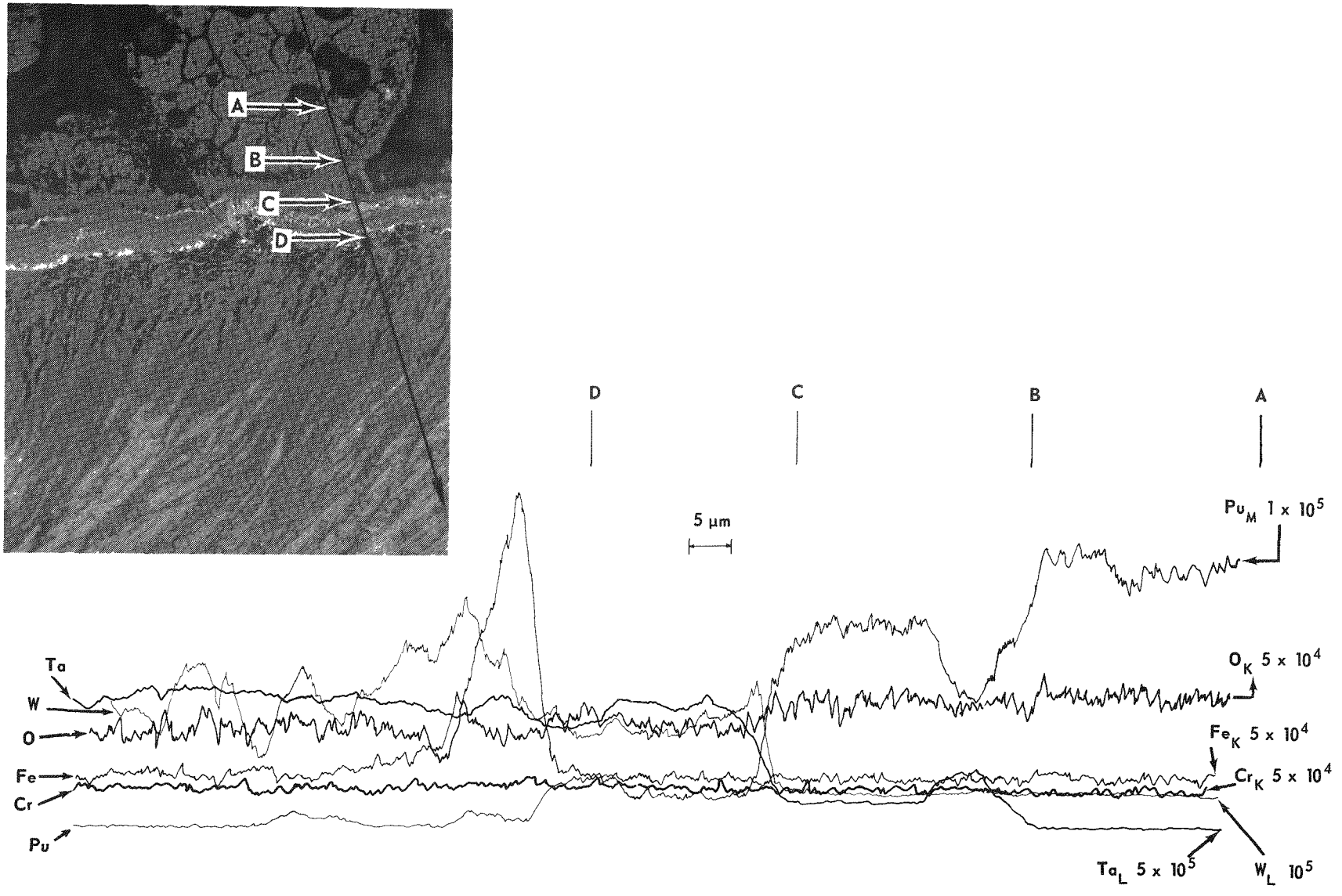

FIGURE 6 - Electron microprobe strip chart analysis of the liner alloy-fuel interface in Sample II. Photograph shows areas A, B, C, and D of Sample II interface which is also shown on the strip chart (read from right to left). Photomicrograph 300X

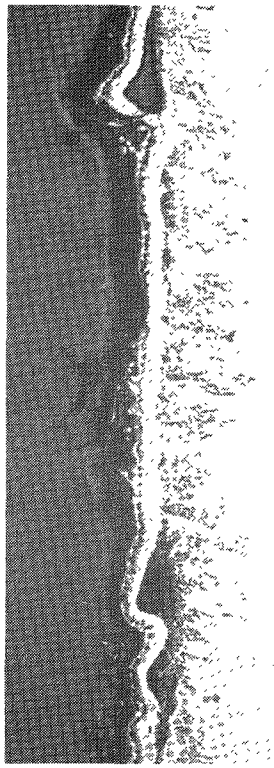

FIGURE 7 - Fuel-liner interface at end of the capsule (sample II area). (130X)

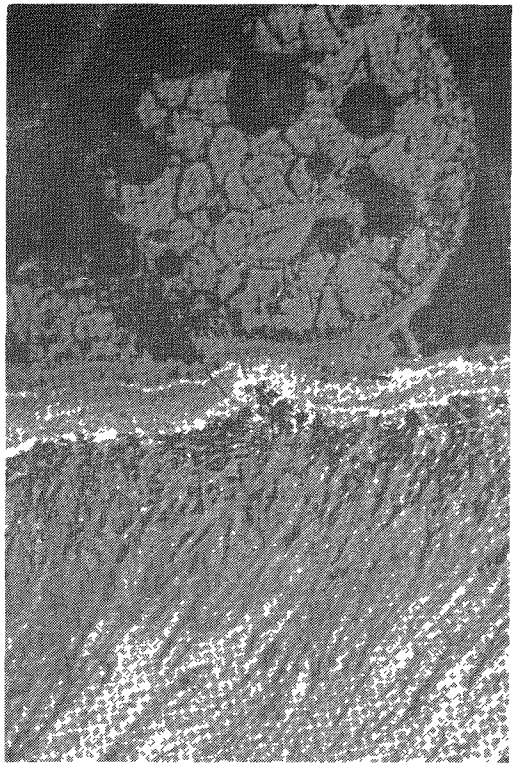

FIGURE 8 - Effect of thermal decomposition at the fuel-liner interface. (300X)

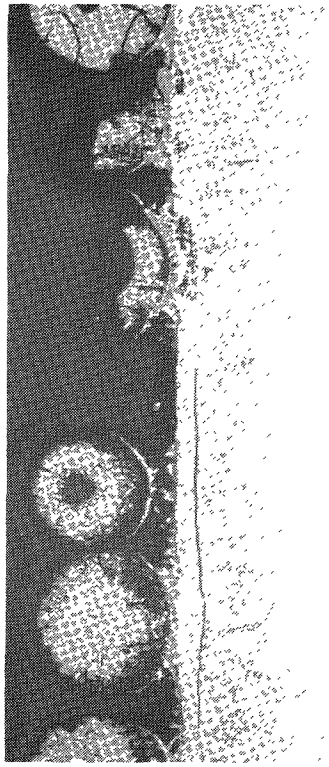

FIGURE 9 - Typical region of the fuel-liner interface. (300X)

the interface coupled with the presence of tantalum represents the diffusion of tantalum into the fuel particle. This layer is also about 25 μm thick. In addition, a small amount of plutonium is seen associated with the iron peak between 25 and 35 μm from the interface. The buildup of tungsten at the interface seen in Figure 6 results from the depletion of the tantalum from the liner resulting from reaction with oxygen from the thermal decomposition of the plutonium dioxide fuel. The effects of this thermal decomposition on the fuel can be seen in the photomicrograph of Figure 8 as a small needle-like phase within the microsphere. This phase is indicative of substoichiometric fuel, PuO_{2-x}. It can also be seen that the iron impurity in the fuel diffused into the liner. Interaction of the iron with the tungsten is suggested by the coincidence of the traces of these two elements at 25-30 μm from the interface. The gray stringers extending through the base metal are probably Ta_2O_5 resulting from oxidation along preferential diffusion paths such as grain boundaries. The black elongated artifacts in Figure 6, region D appear to be a phase which pulled out during metallographic preparation so that positive identification could not be made. However, it should be noted that this region is richer in impurities than regions on either side.

The area shown in Figure 8 contains more of this black pulled-out phase than other areas and represents about 10% of the total interface. A typical region is seen in Figure 9 which is similar to Figure 7. The fine gray stringers represent the tantalum oxide as discussed previously. The microprobe trace is shown in Figure 10. A total reaction area of 50 μm can be seen. According to the x-ray strip chart analysis the white area (region D, Figure 6) is high in tungsten. Its metallic appearance suggests this area is unreacted tungsten-tantalum alloy, since some tantalum is also present. No impurities were detected along this trace which supports the conclusion that the black particles are associated with the fuel impurities.

Photomicrographs were taken at different magnifications along the fuel-liner side wall interface, (Sample III in Figure 5b) and are shown in Figure 11. A trace of the microprobe strip chart and photomicrograph of the large white reaction product are shown in Figure 12. A plutonium-tantalum reaction product of 22 μm wide is seen near the surface. The trace also shows that the fuel impurities penetrated the liner 120 μm. Figure 12, Area A on the photomicrograph, is the outer dark band and is a reaction between plutonium and tantalum as well as other mixed reaction products. The major white phase in Figure 12, Area B is a mixture of cobalt, chromium, and iron intermetallics. The gray phase at the inner edge of Area B is richer in nickel and tungsten. The cobalt peaks in the strip chart trace show that Area C contains iron, cobalt, nickel and tungsten. The iron, chromium, cobalt and nickel are present as impurities in the fuel as shown in Table 1. No reason can be given for the spasmodic concentration of these impurities along the interface, unless the impurities are not homogenously distributed throughout the fuel. The increase in the oxygen trace in Area D shows the dark fine stringers to be rich in oxygen.

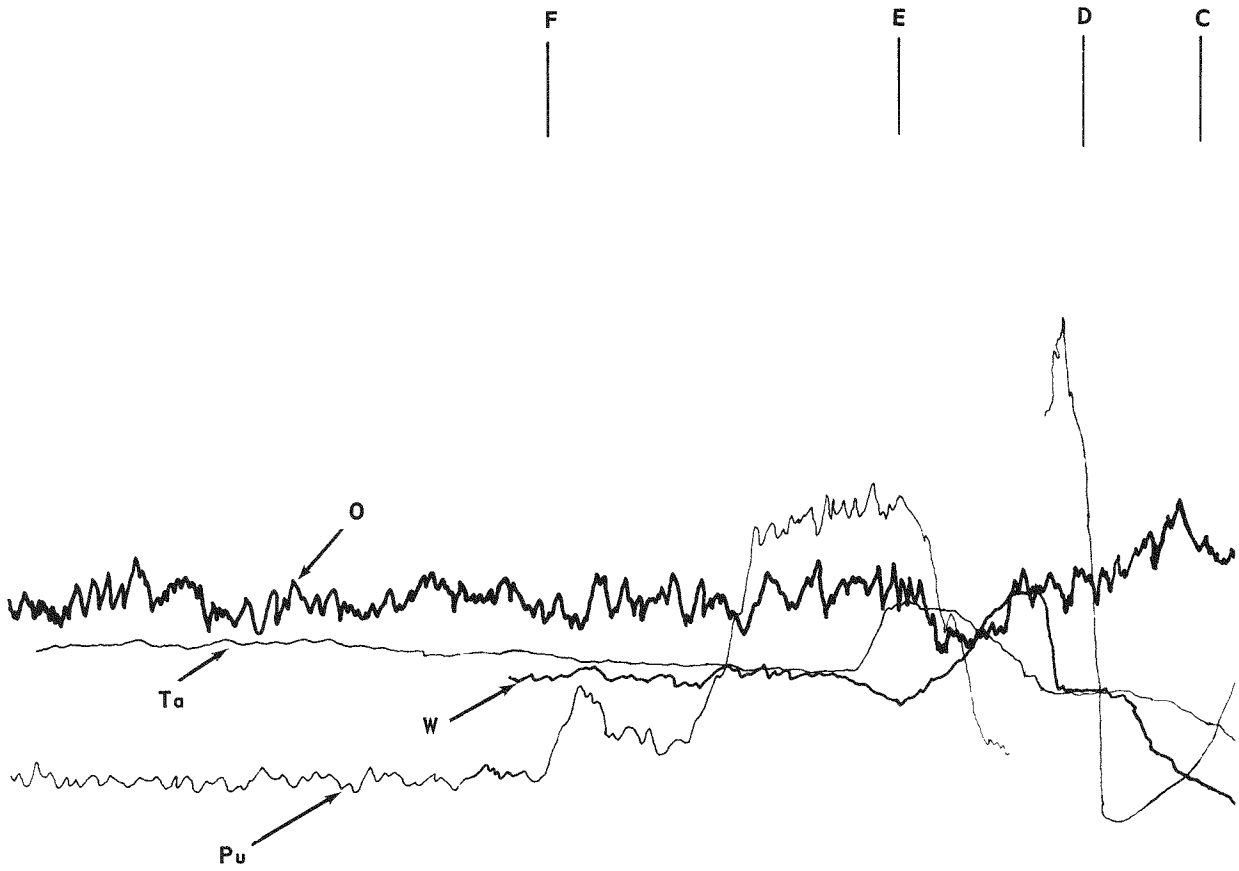

FIGURE 10 - Continued (read from right to left).

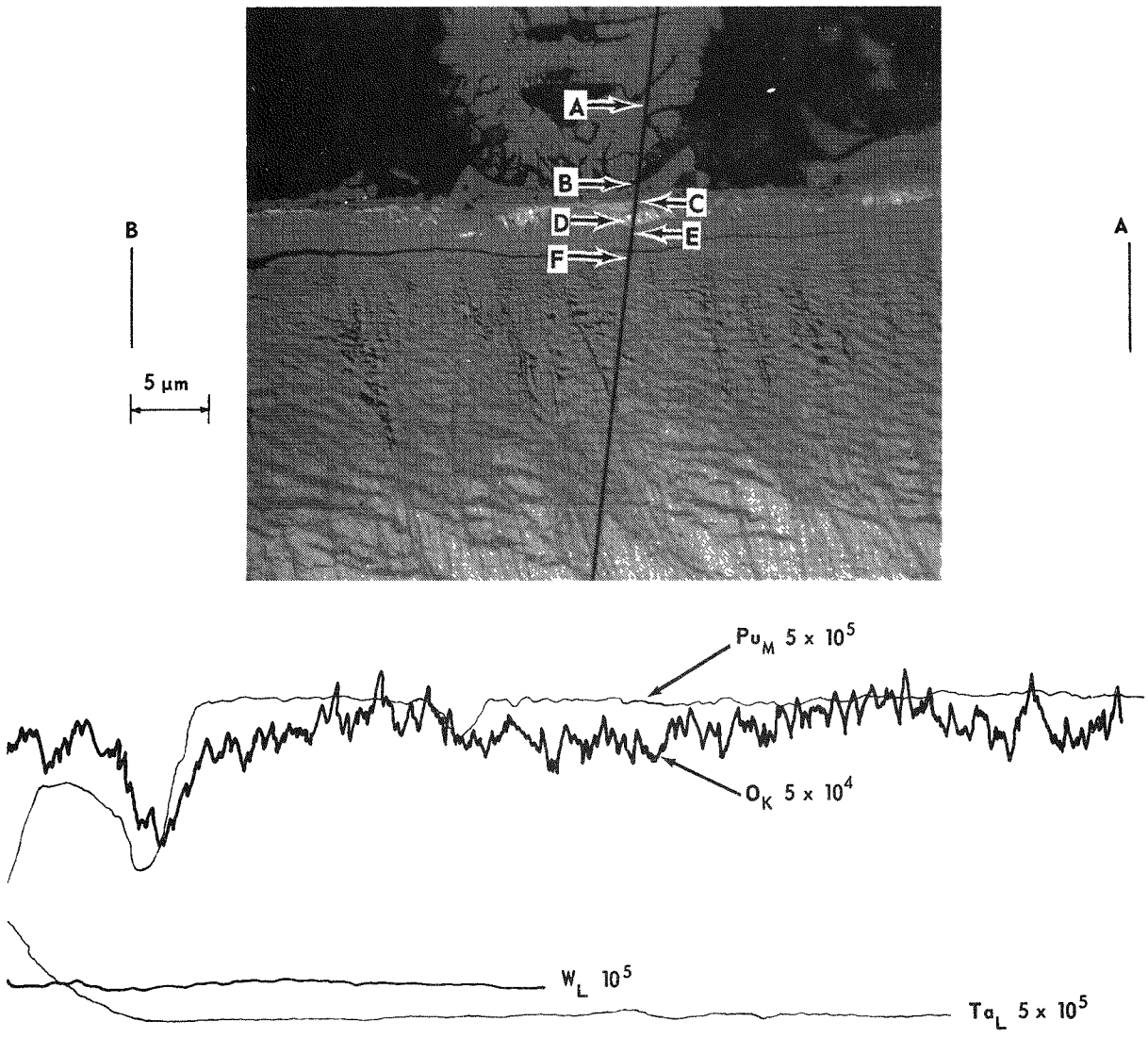

FIGURE 10 - Electron microprobe strip chart of typical fuel-liner reaction interface of Sample I. Photomicrograph 300X

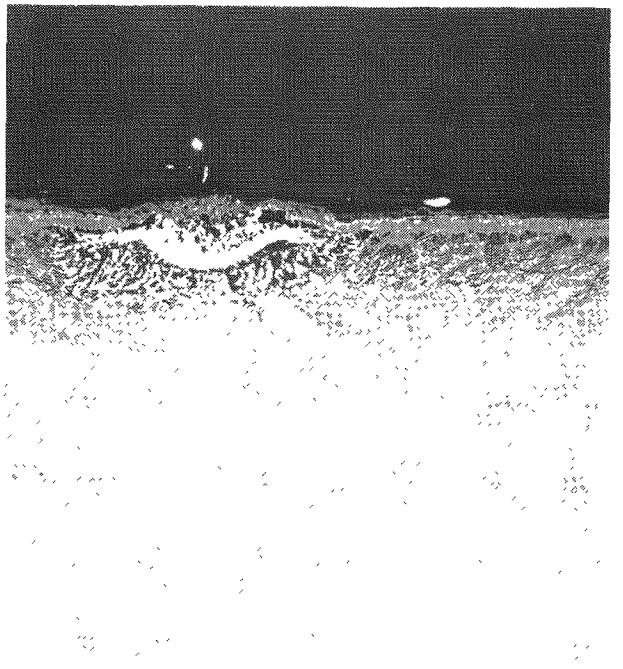

(A) Unetched, 130X

(B) Unetched, 300X

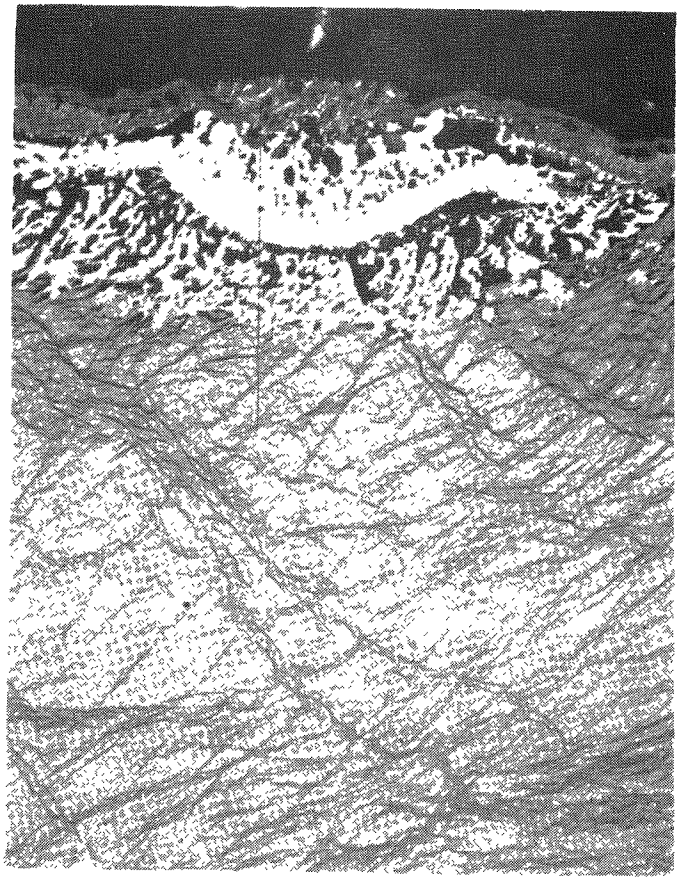

FIGURE 11 - Photomicrograph of fuel-liner side wall interface showing large impurity reaction product from Sample III.

Microhardness data of samples from the end and side of the capsule liner shown in Figures 13 and 14 show that there is an appreciable hardness increase in the Ta-10W alloy because of the absorbed oxygen and the formation of tantalum oxide stringers. From these photographs it can be seen that the brittleness of the edge reaction area caused cracking when the microhardness was done giving inconsistencies in the curve. No attempt was made to select specific areas for each measurement. The black areas, which appear to be a pulled out phase, could not be identified. Measurements made on these regions appear to be softer than adjacent regions, suggesting the absence of material below the indentation. The Ta-10W alloy was obviously embrittled as indicated by the high microhardness values. The hardness of the starting material was about 260-280 VHN (Vickers Hardness Number).

Fin-Fuel Interface - A typical area of the tantalum-10% tungsten alloy fin-fuel interface is seen in Figure 15. The area microprobed is seen in Figure 16 along with its corresponding strip chart trace. Area A is a piece of plutonium fuel as verified by the high plutonium trace followed by its corresponding oxygen trace. Some tantalum is also present in this layer. Area B is seen as the gray band with the white inclusions in the photomicrograph. The strip chart trace shows that the white inclusions are tungsten rich in a matrix of plutonium-tantalum reaction products. Rough calculations indicate this dark gray phase to be $PuO_2 \cdot 2Ta_2O_5$. The high cobalt, nickel, iron, and chromium and tungsten peaks in Area C indicate the presence of intermetallics. These compounds extend from 75 to 170 μm into the fin. The high microhardness values shown in Figure 17 plus the oxygen found in the strip chart trace shows that intergranular phase is an oxide phase, presumably Ta_2O_5. It is obvious that the fin has become oxidized to a much greater extent than the liner. No doubt this is due to the fact that the fin is in closer proximity to more oxygen than the liner, as well as the temperature being higher at the fin.

Liner Strength Member Interface - A photomicrograph of the tantalum-10% tungsten liner-TZM strength member interface can be seen in Figure 18. The tantalum oxide stringers can be seen extending completely through the liner to the strength member. The strip chart trace in Figure 19 shows a 10 μm diffusion zone between the molybdenum in the strength member and the tantalum in the liner. Where the tantalum diffused into the TZM at the interface, a tungsten buildup is shown in the strip chart trace because the tantalum was depleted from the liner. The presence of oxygen in the liner is seen as a slight increase of O_2 on the strip chart trace on the liner side. Also, the slight increase in the background along with the hardness data in Figure 20 of the oxygen trace suggests solution of oxygen in the tantalum alloy.

The morphology of the tantalum oxide stringers suggests the oxygen diffused down short circuiting paths. These short circuiting paths could either be grain boundaries or dislocations. Distortion of the metal near the surface, probably by the machining step, is indicated by the change in orientation of the stringers at the interface.

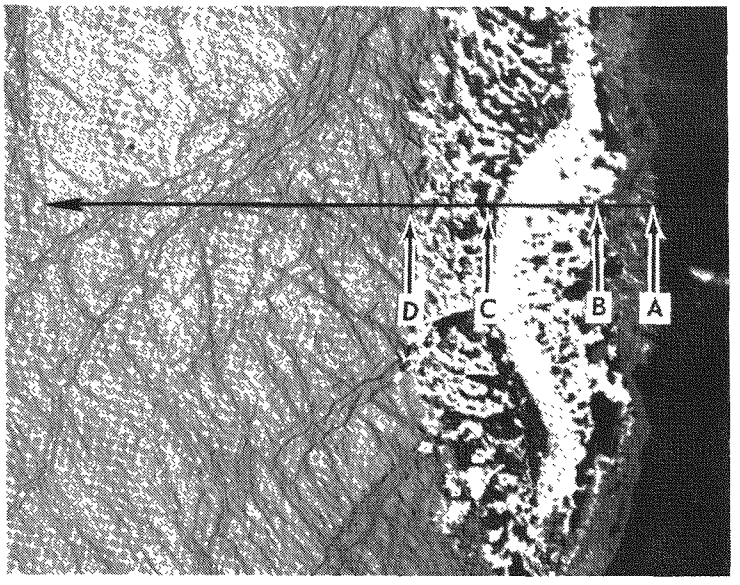

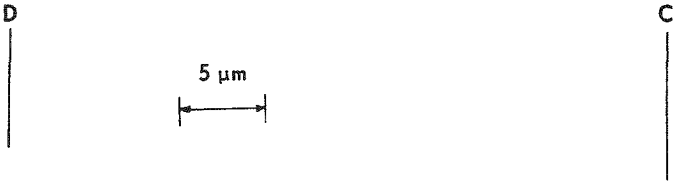

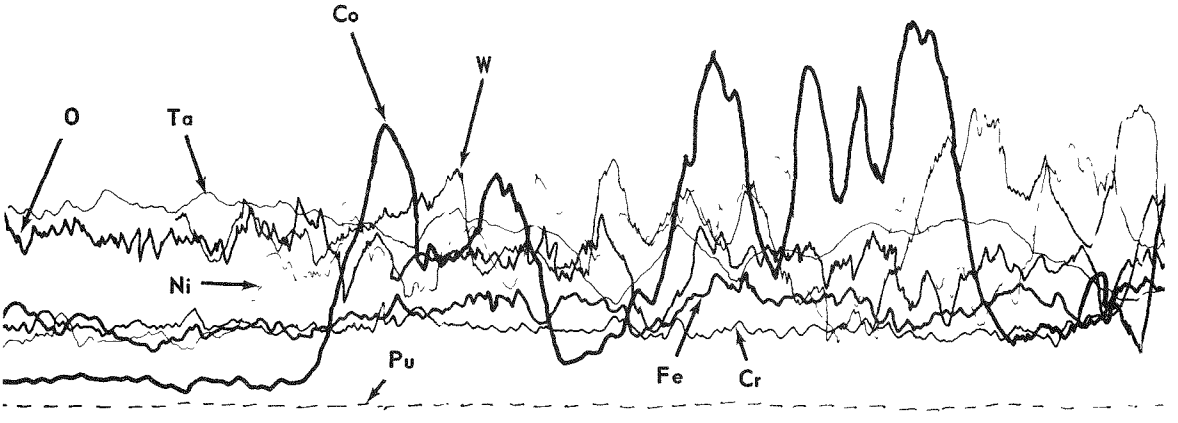

Figure 12 - Continued (read from right to left).

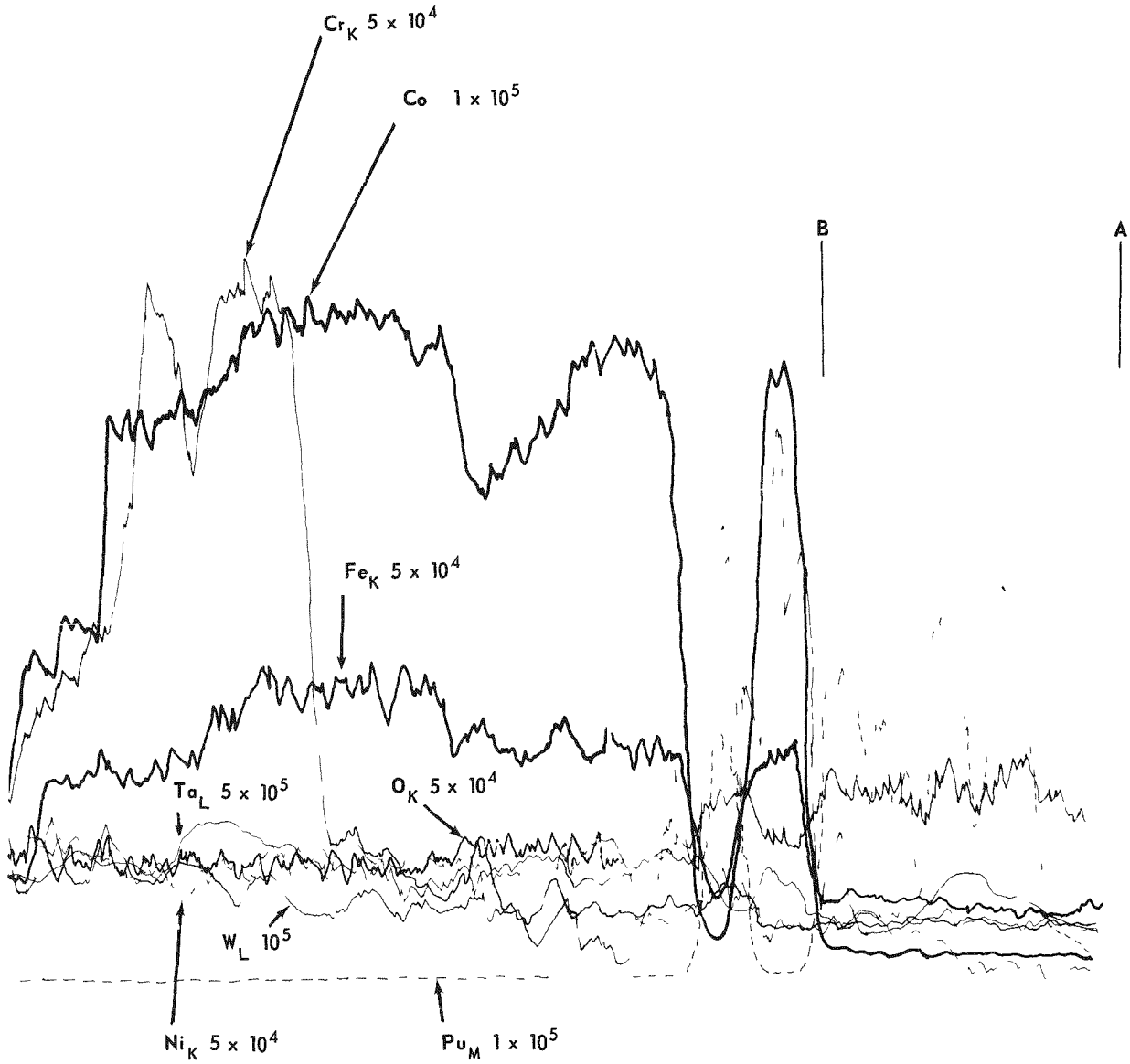

FIGURE 12 - Electron microprobe strip chart of large impurity reaction product from Sample III.

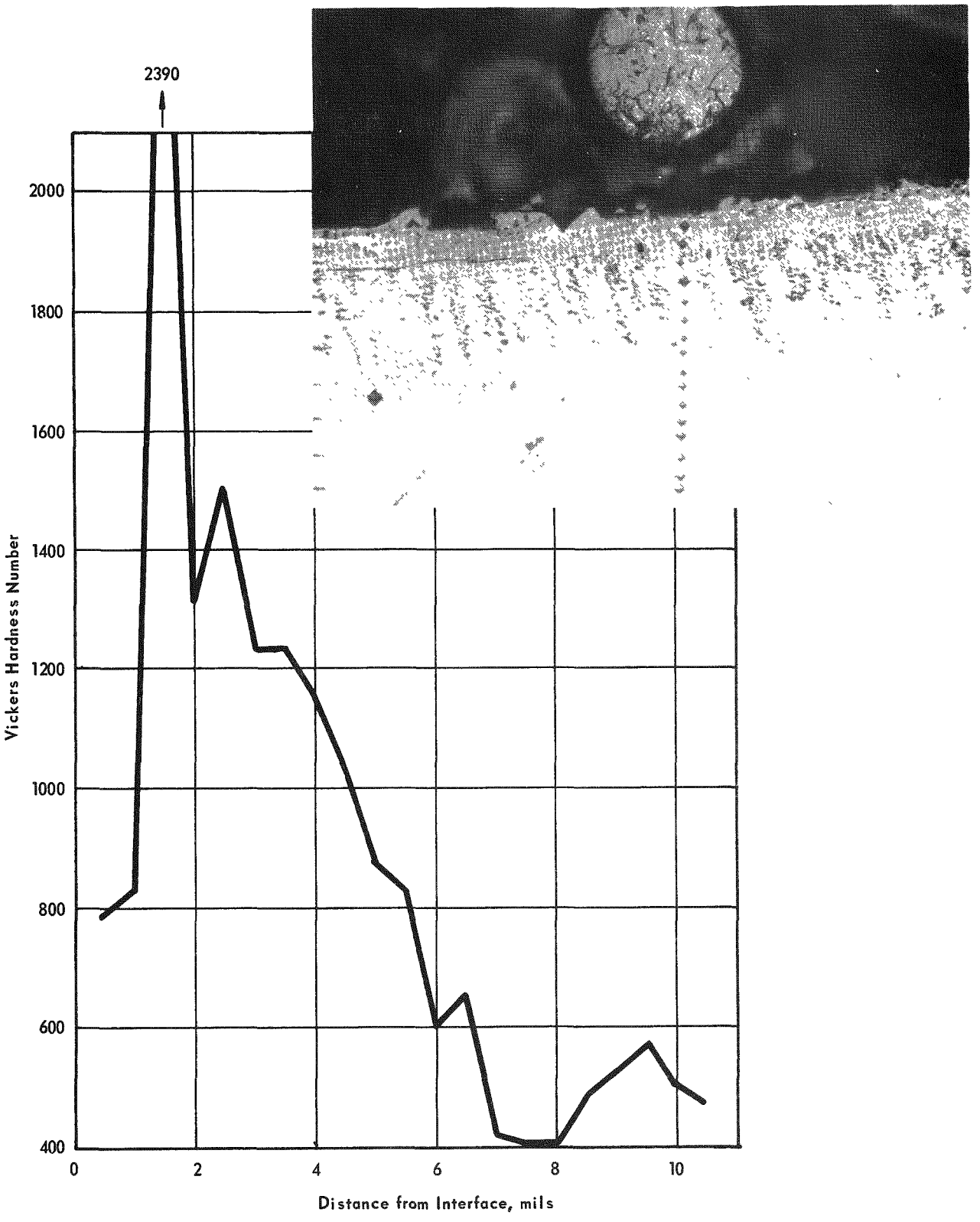

FIGURE 13 - Microhardness traverse from Sample I fuel-liner interface.

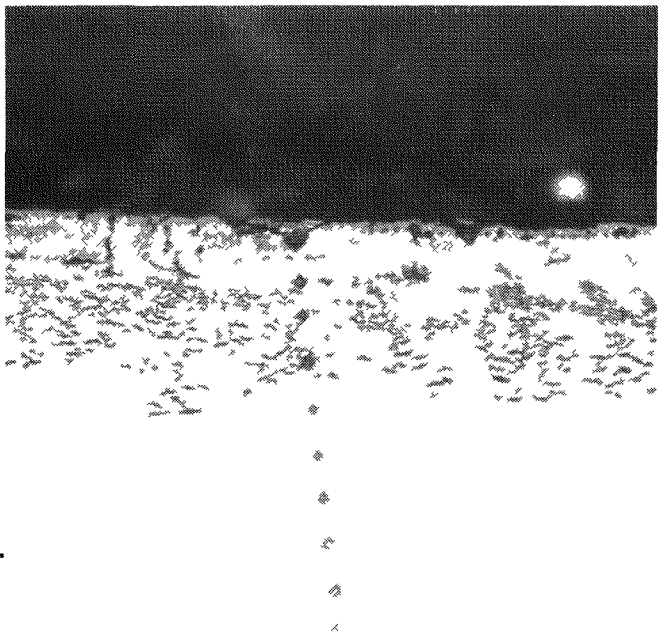

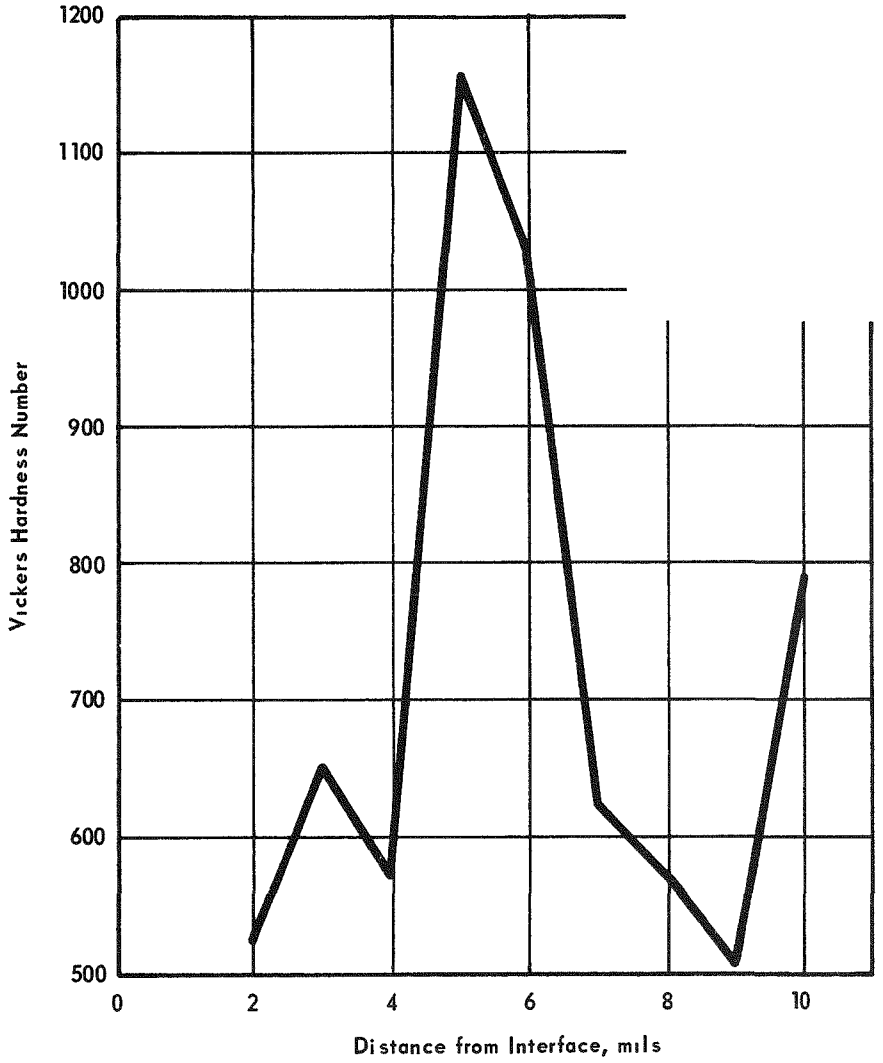

FIGURE 14 - Microhardness traverse from Sample III fuel-liner interface.

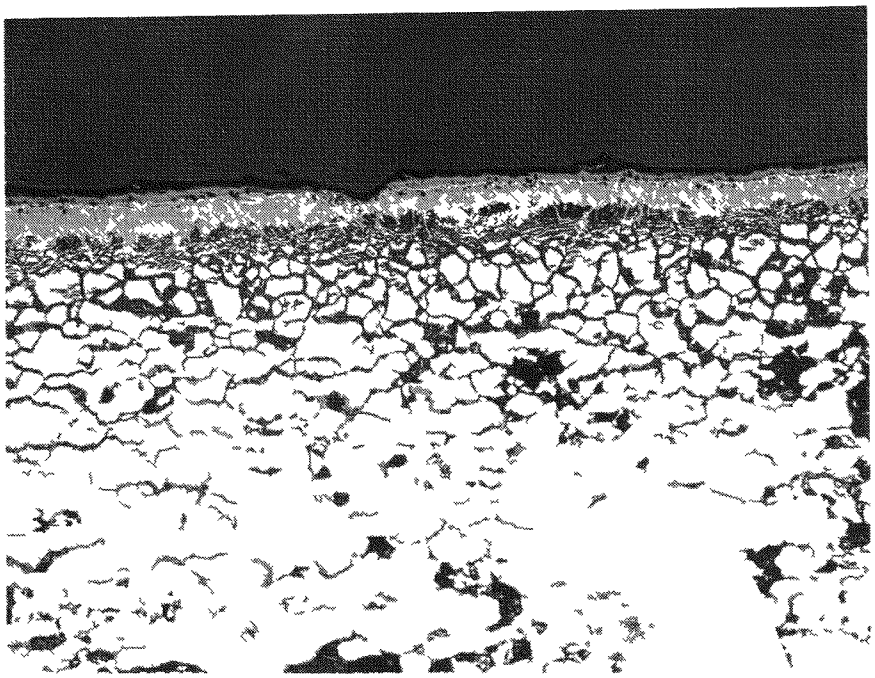

FIGURE 15 - Typical photomicrograph of the fin-fuel interface.

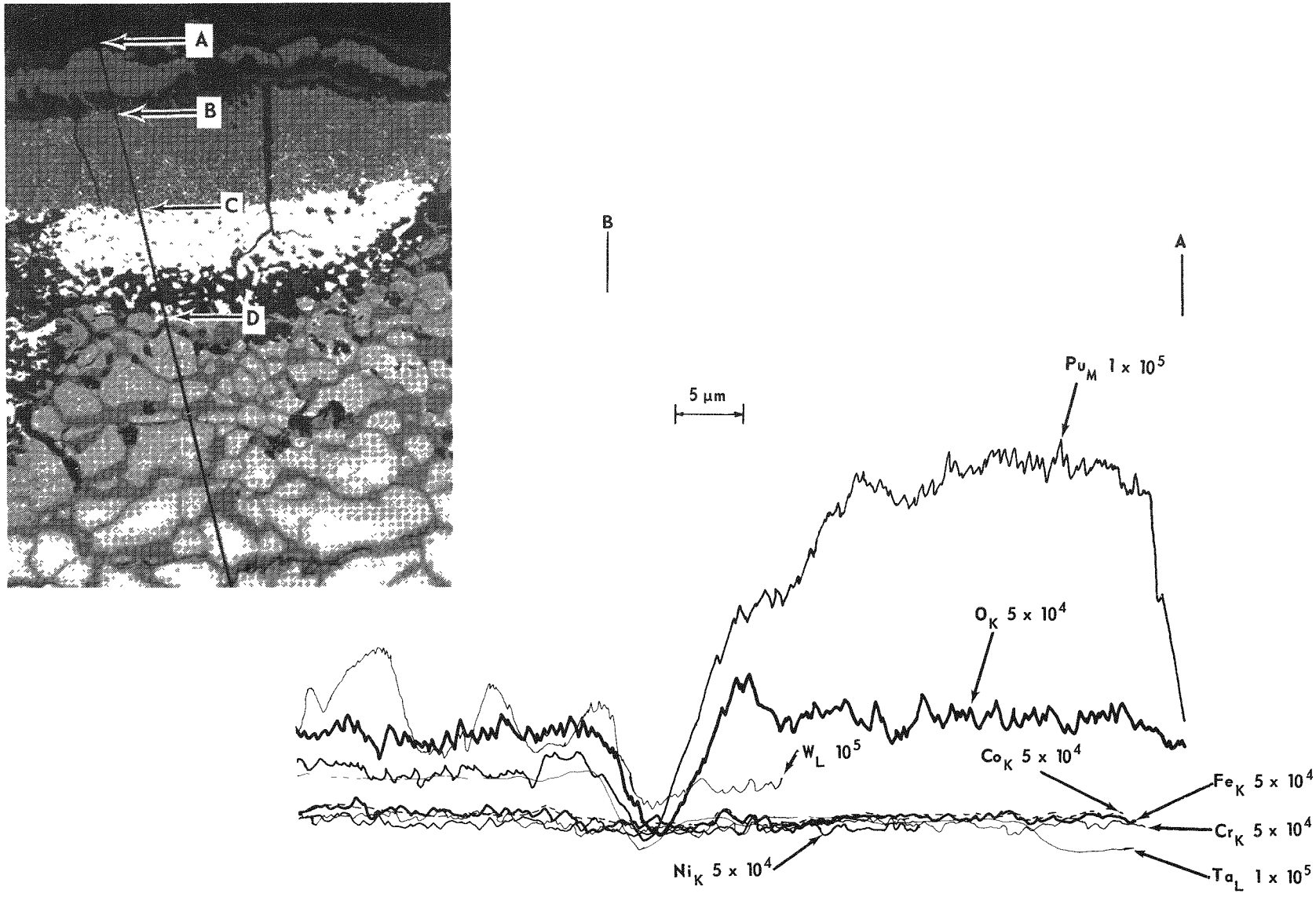

FIGURE 16 - Electron microprobe strip chart analysis of region along the fin-fuel interface, (read from right to left). This chart is continued on the following page.

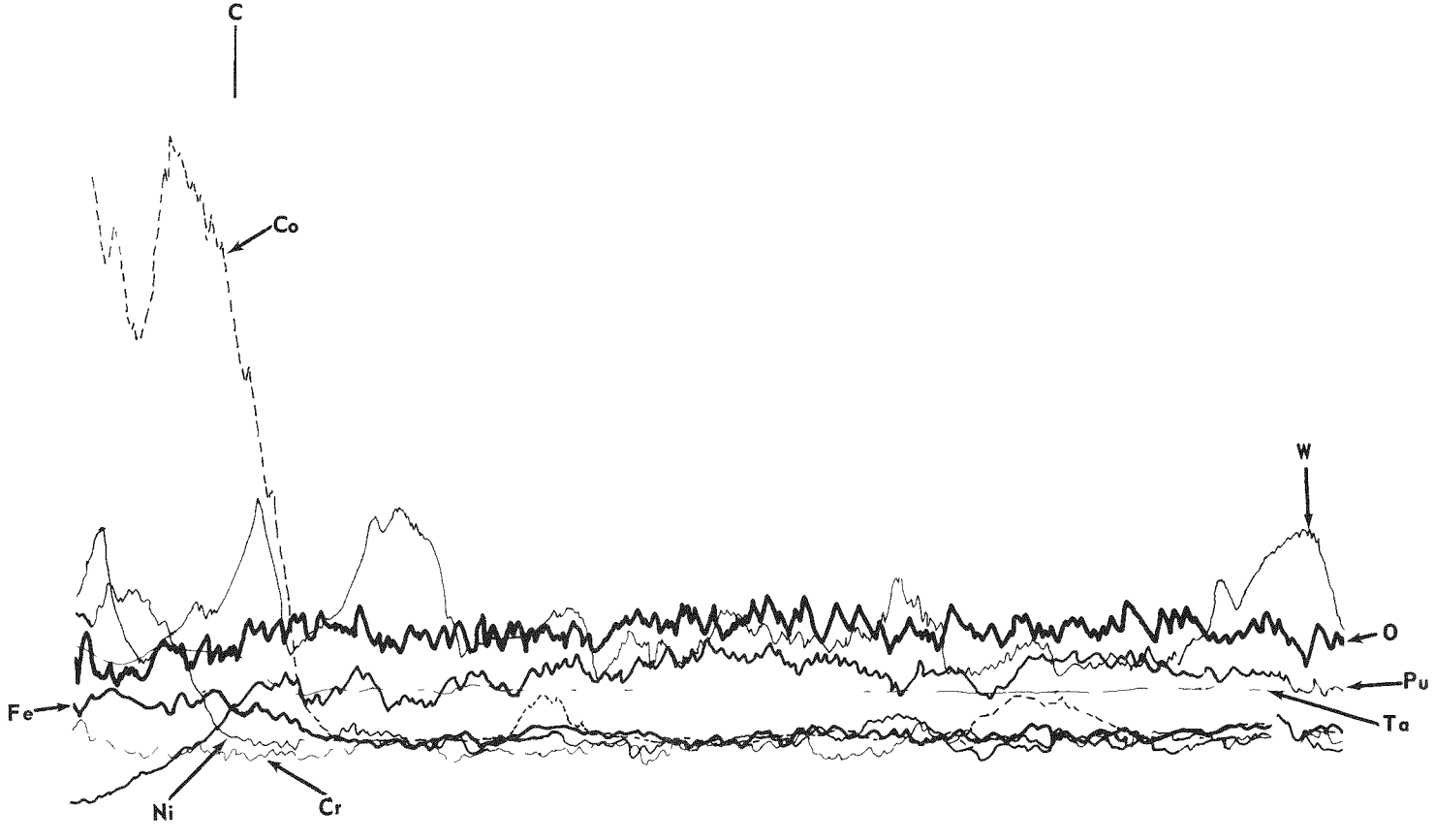

FIGURE 16 - Continued (read from right to left).

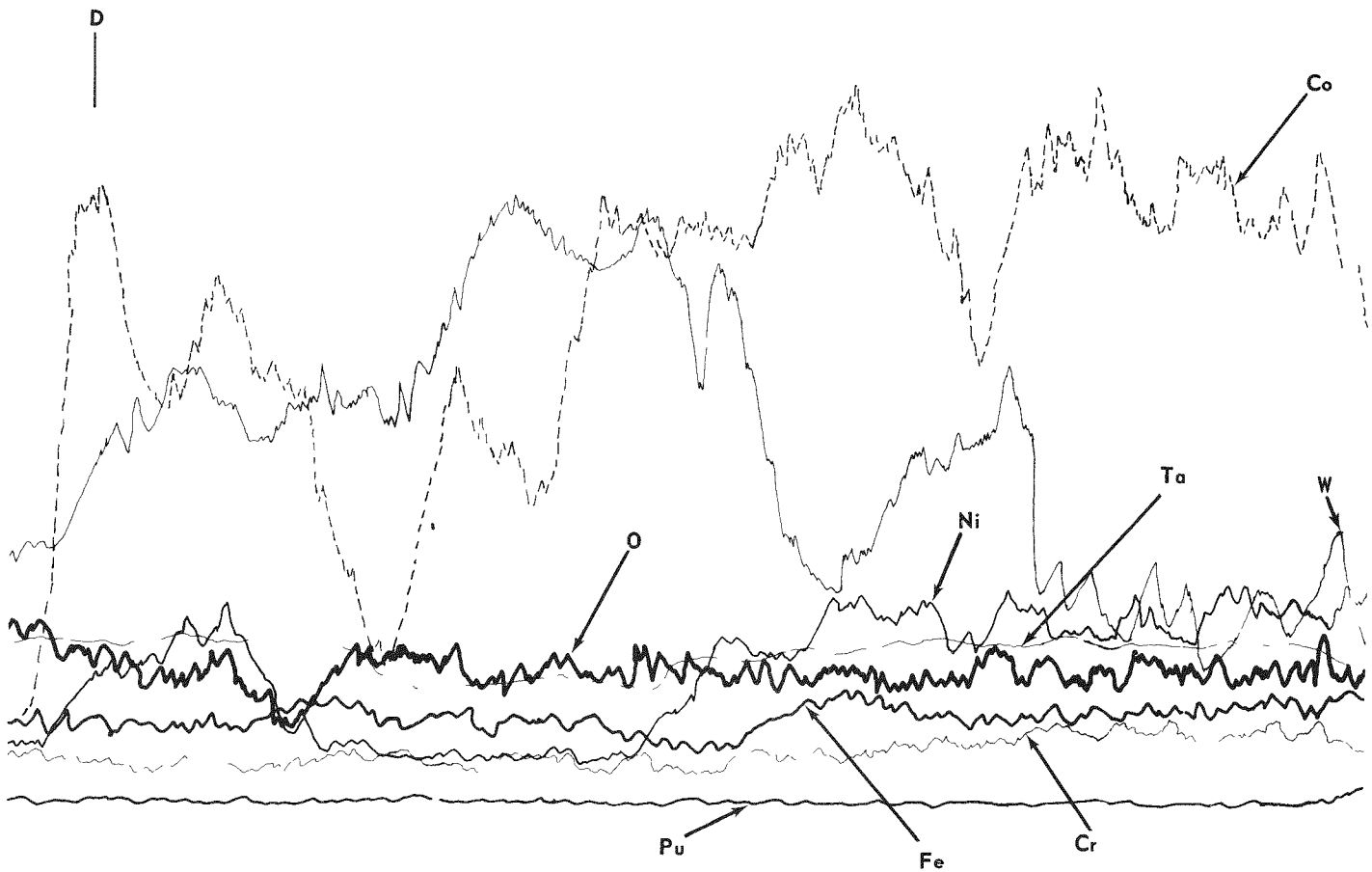

FIGURE 16 - Continued (read from right to left).

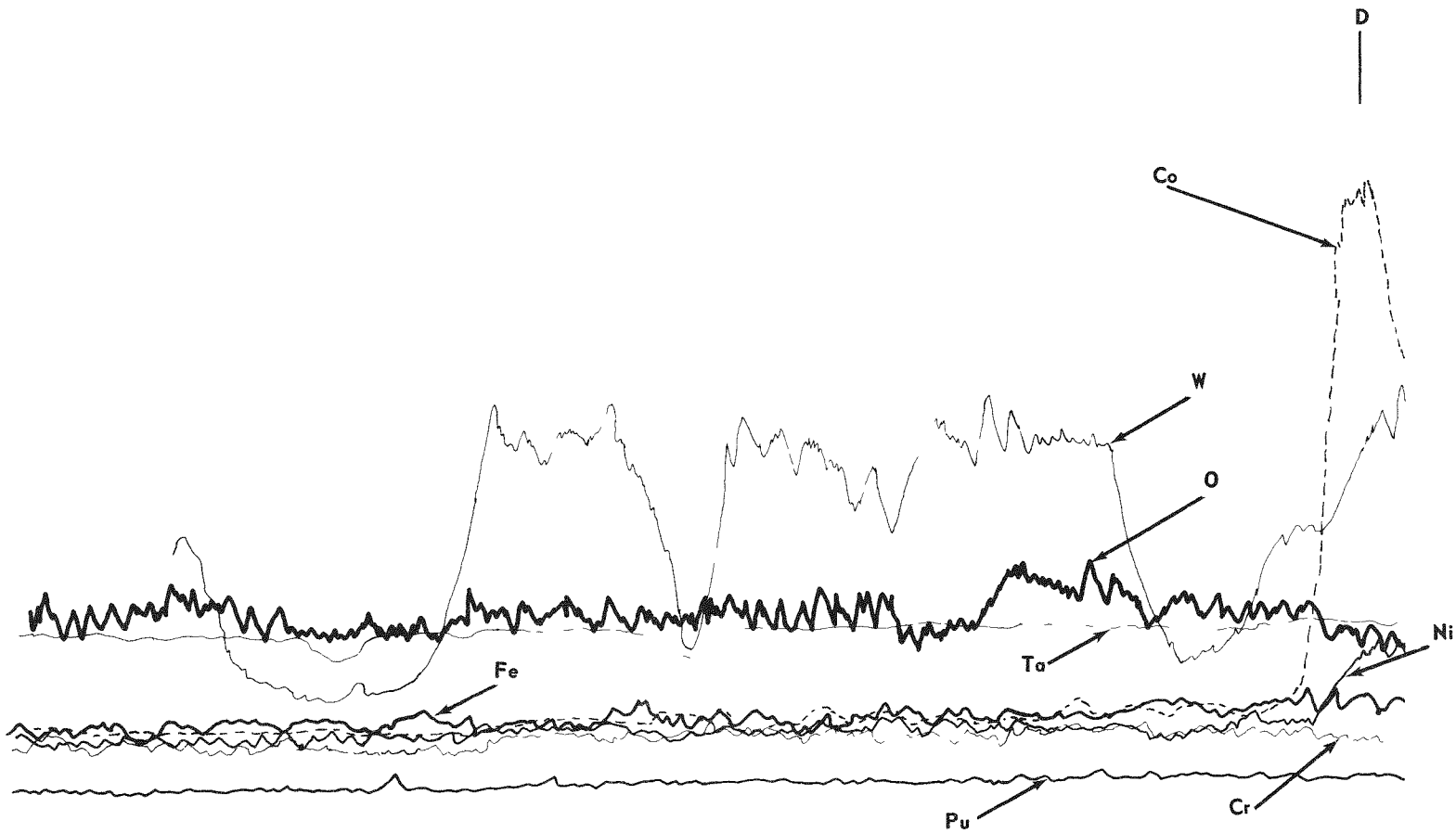

FIGURE 16 - Continued (read from right to left).

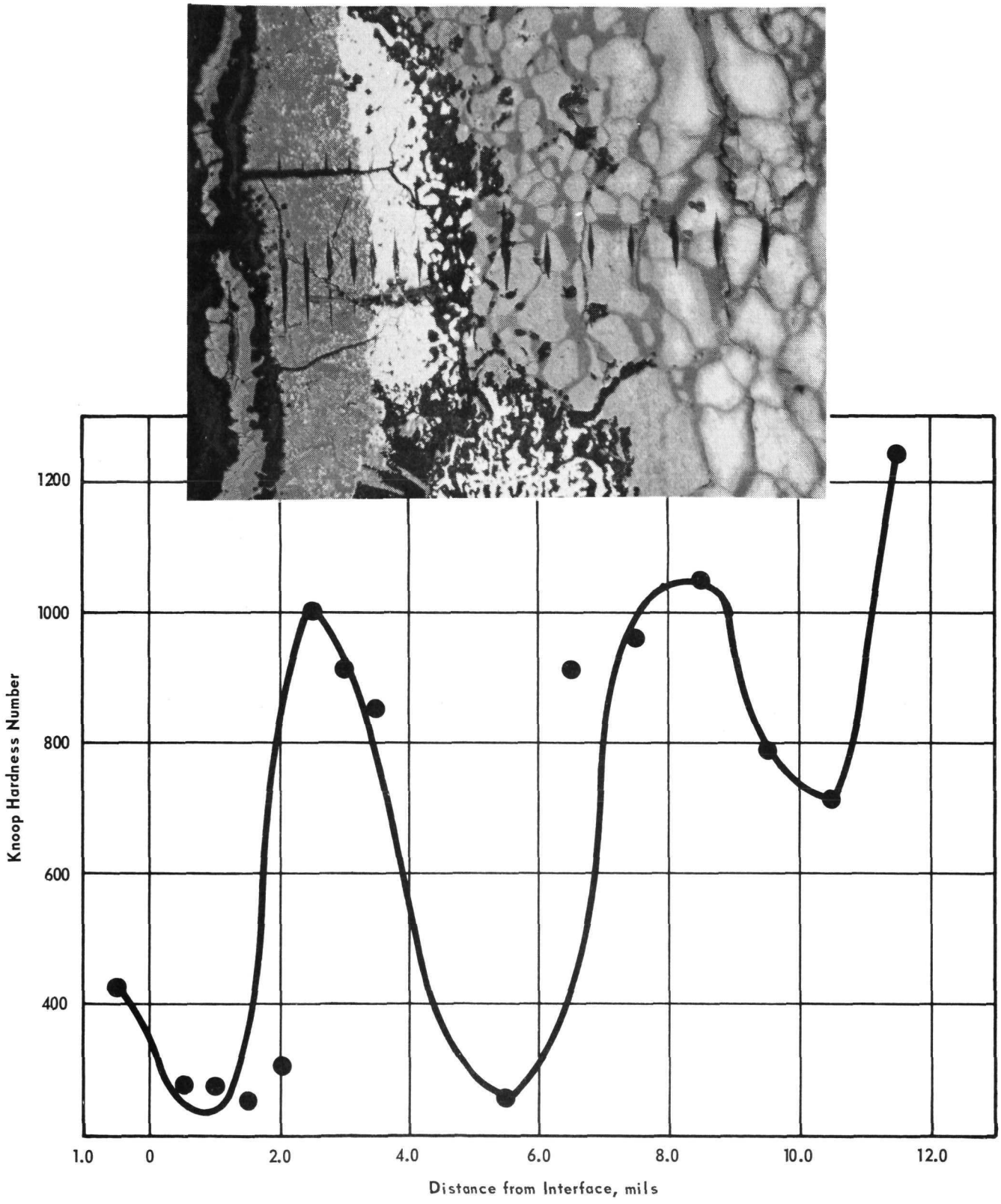

FIGURE 17 - Microhardness traverse from center fin across impurity reaction product.

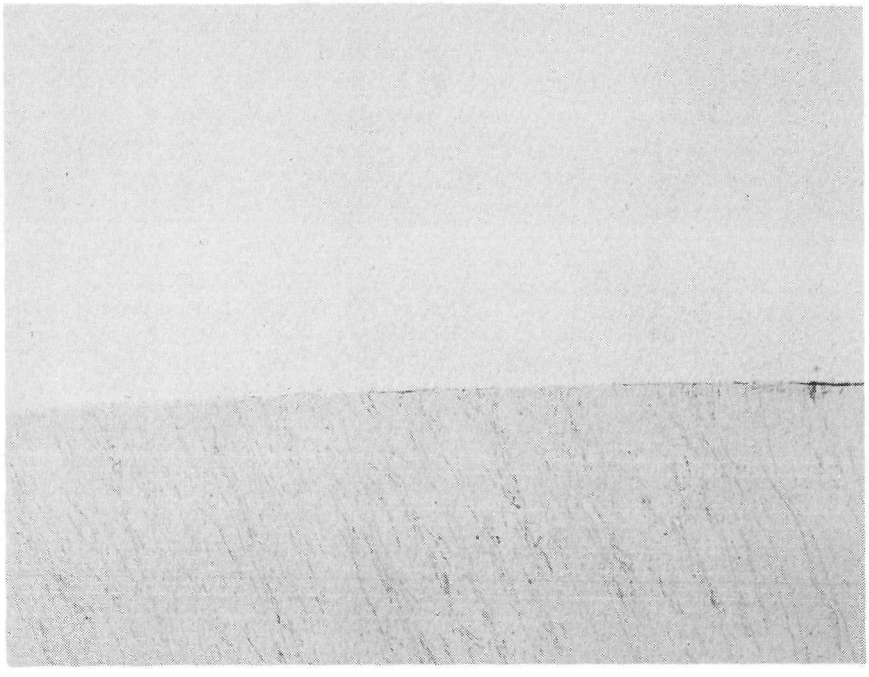

FIGURE 18 - Photomicrograph of liner-strength member interface. Unetched, 130X

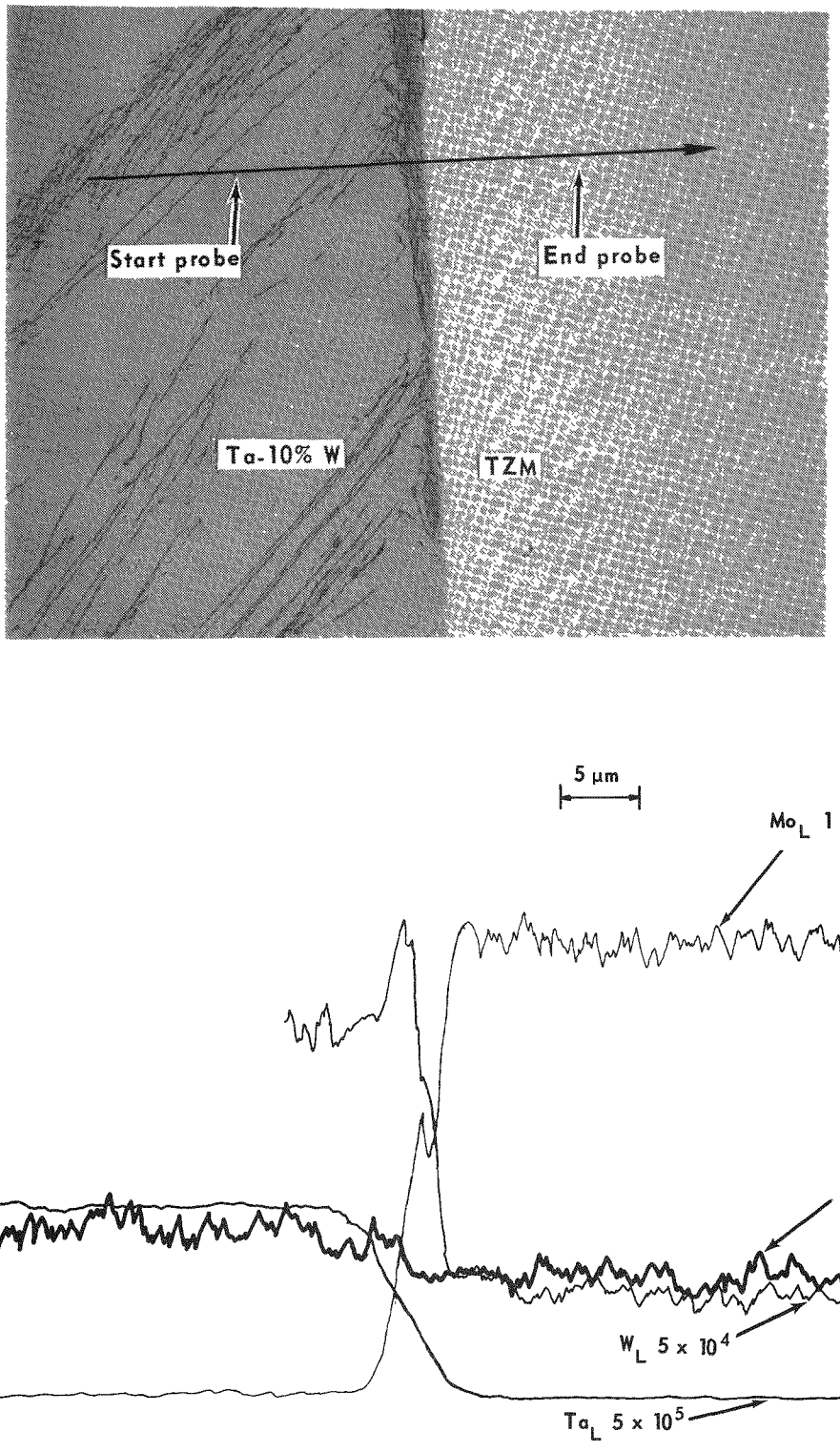

FIGURE 19 - Electron microprobe strip chart of liner-strength member interface. Photomicrograph 300X.

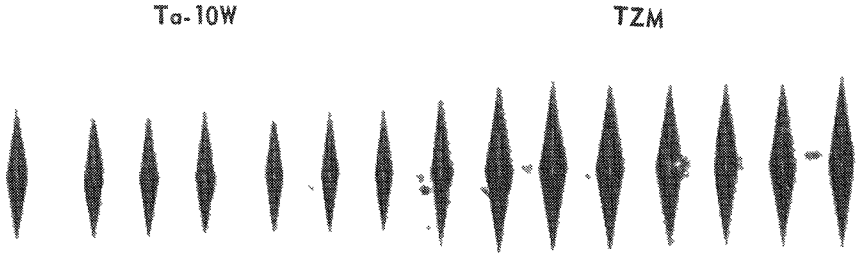

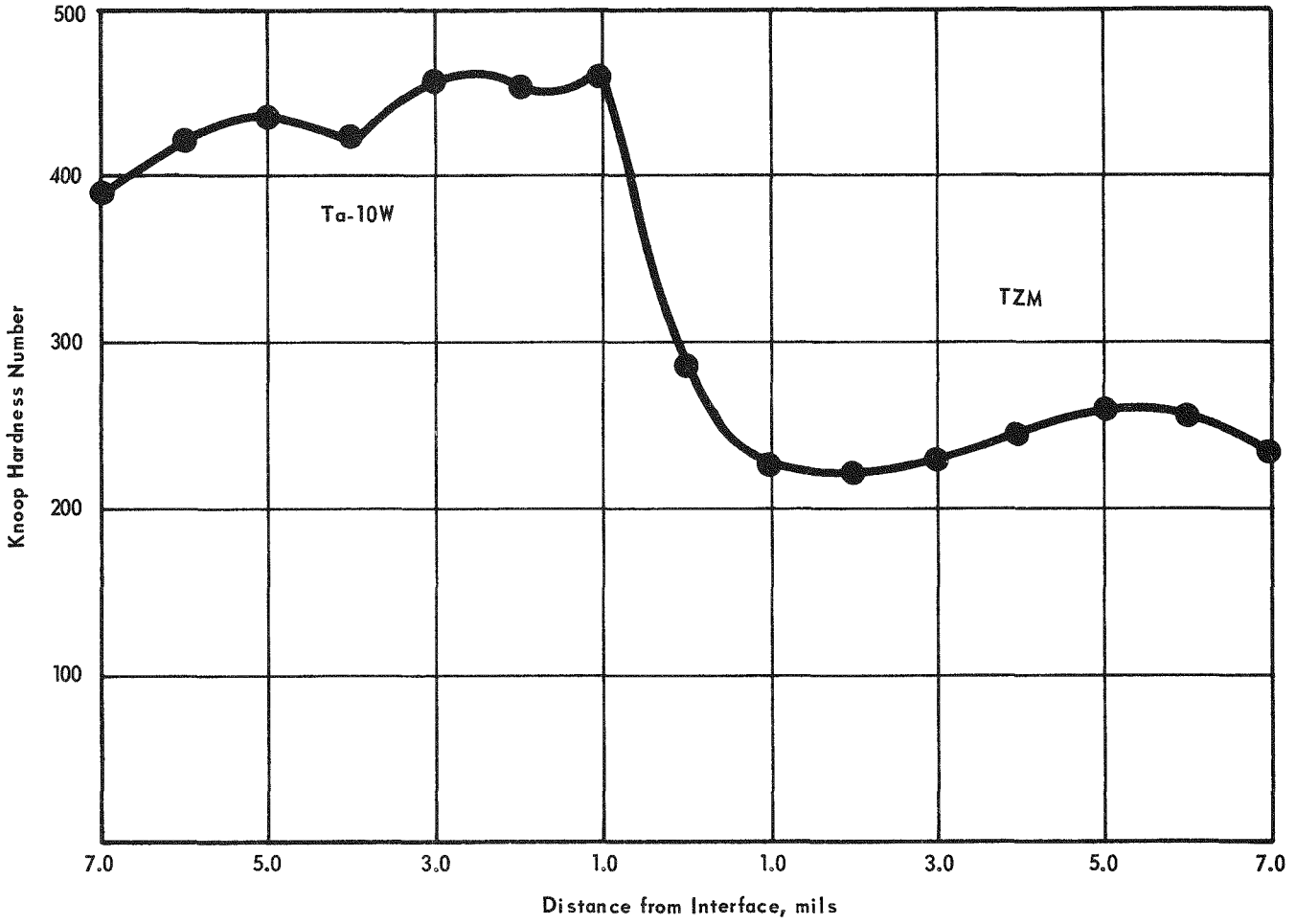

FIGURE 20 - Microhardness traverse across the liner-strength member interface. Photomicrograph 300X.

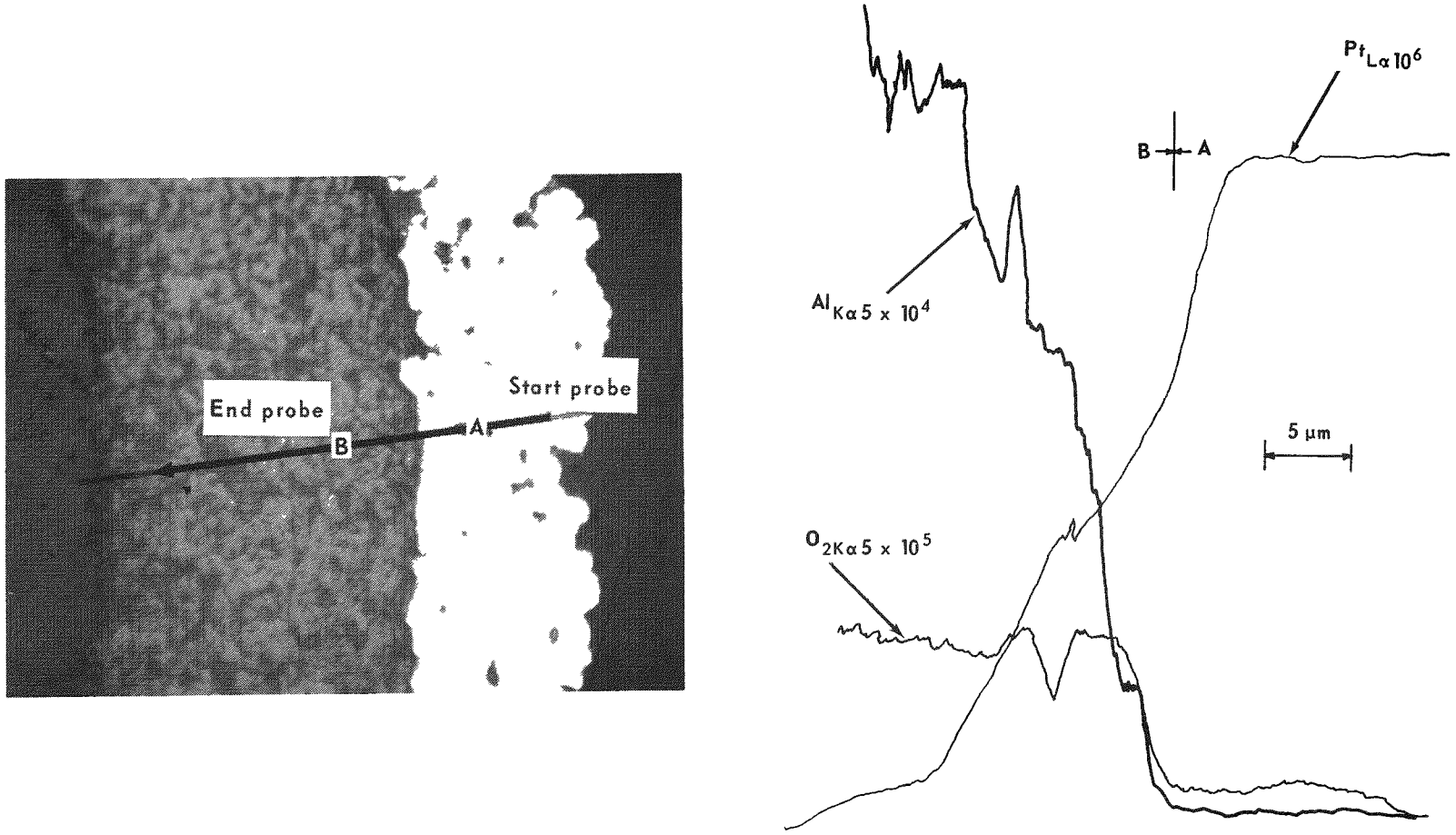

FIGURE 21 - Photomicrograph and electron microprobe strip chart analysis of the platinum-aluminum oxide interface.

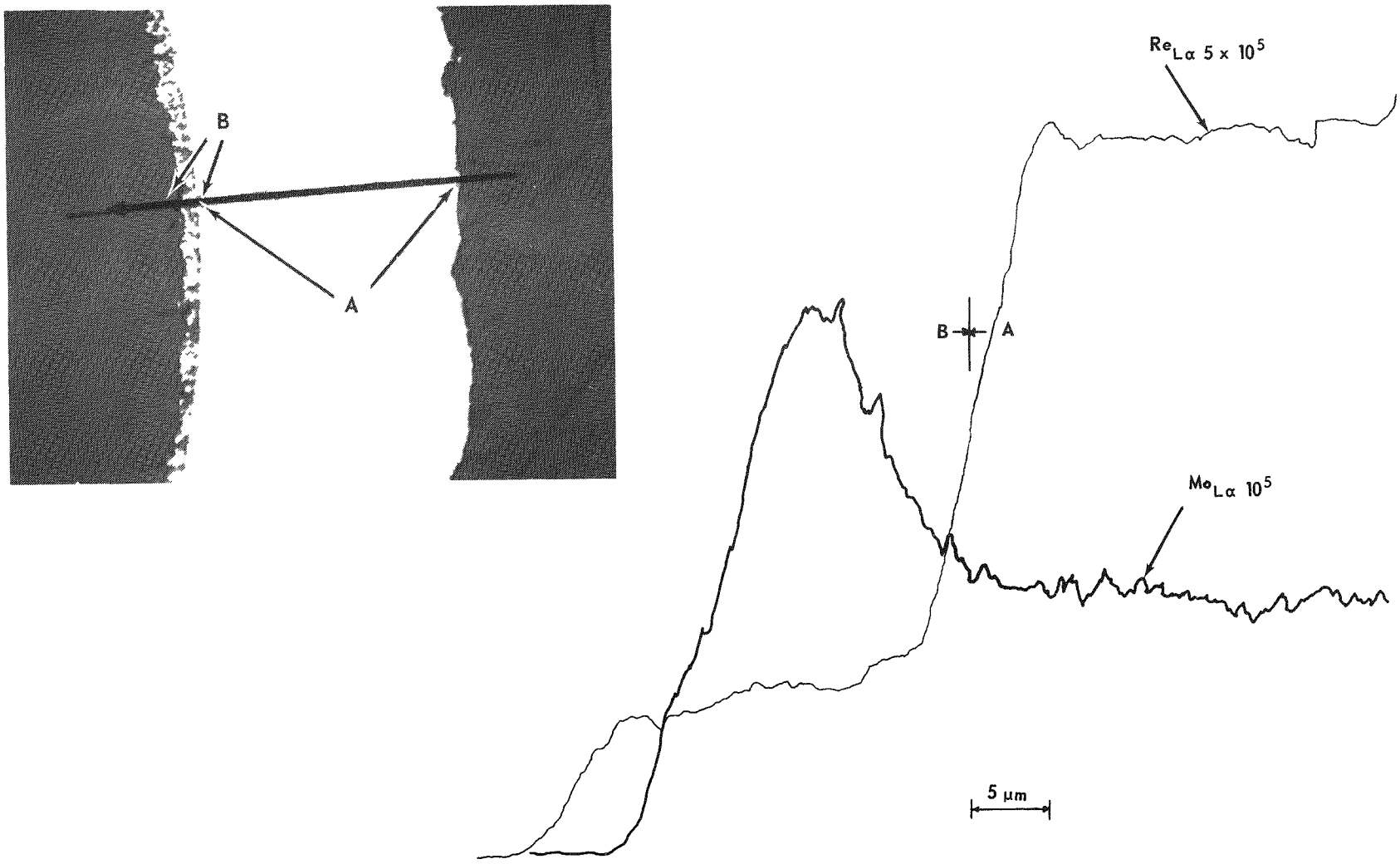

FIGURE 22 - Electron microprobe strip chart analysis and photomicrograph of molybdenum-50% rhenium coolant tube.

Platinum Cladding - Aluminum Oxide Interface The TZM was clad with platinum which had been coated with aluminum oxide. The platinum cladding separated from the TZM and no interface was examined. The platinum-aluminum oxide interface showing the white platinum layer is shown in Figure 21. This photomicrograph illustrates the porosity of the aluminum oxide spray coating. The strip chart of Figure 21 shows a 20 μm reaction layer between the platinum cladding and the coating.

Molybdenum-50% Rhenium Ammonia coolant in the flow tube reacted with the rhenium leaving a depletion of rhenium and an increase of molybdenum as seen in the strip chart trace, Figure 22.

CONCLUSIONS

From this investigation the following conclusions can be drawn:

- Plutonium and tantalum reactions were found in all fuel liner interface areas.
- The fuel impurities diffused into the Ta-10W liner although no adverse results were noticed.
- Reaction with oxygen, resulting from decomposition of the fuel, with the tantalum-10% tungsten alloy results in tantalum oxide stringers and hardness increases due to solution of the oxygen.
- Oxidation in the internal fin was much greater than in the liner.
- The ammonia coolant reacted with the rhenium in the cooling tubes, resulting in depletion of rhenium from the alloy.
- Interaction between the platinum clad and the Al_2O_3 coating was observed.
- Some substoichiometry was observed in the microspheres adhering to some of the samples.

ACKNOWLEDGEMENTS

The authors wish to acknowledge the assistance of Mr. D. L. Roesch in performing the electron microprobe analyses.

Paul F. Carpenter, Editor